JOURNAL OF COMPUTATIONAL PHYSICS 25, 1–31 (1977)

A Numerical Study of 2-D Turbulence

BENGT FORNBERG

California Institute of Technology, Department of Applied Mathematics, Pasadena, California 91125

Received June 17, 1976; revised December 10, 1976

A simulation of 2-D turbulence in a square region with periodic boundary conditions has been performed using a highly accurate approximation of the inviscid Navier–Stokes equations to which a modified viscosity has been added. A series of flow pictures show how a random initial vorticity distribution quickly assumes a stringlike pattern which persists as the flow simplifies into a few "cyclones" or "finite area vortex regions". This trend towards well-defined large-scale structures can make it questionable if the 2-D flow should be described as "turbulent" and it casts some doubts on the concept of inertial range and the relevance of energy spectra. The change in appearance seems to be associated with a buildup of phase correlations in the Fourier representation of the vorticity field. During this initial buildup, the energy spectrum seems to follow a k^{-3}-law, but this behavior does not persist. If there is a power law for steady turbulence the results suggest that is more likely to be a k^{-4}-law.

INTRODUCTION

The Navier–Stokes equations for viscous, incompressible 2-D flow expressed in terms of streamfunction ψ and vorticity ω, are

$$\frac{\partial \omega}{\partial t} = \frac{\partial \psi}{\partial x} \cdot \frac{\partial \omega}{\partial y} - \frac{\partial \psi}{\partial y} \cdot \frac{\partial \omega}{\partial x} + \nu \left(\frac{\partial^2 \omega}{\partial x^2} + \frac{\partial^2 \omega}{\partial y^2} \right), \tag{1}$$

$$\omega = -\left(\frac{\partial^2 \psi}{\partial x^2} + \frac{\partial^2 \psi}{\partial y^2} \right). \tag{2}$$

These equations are studied numerically on a square region with periodic boundary conditions. Randomly generated initial conditions provide a simulation of two-dimensional turbulence.

Burger's equation

$$\frac{\partial u}{\partial t} + u \frac{\partial u}{\partial x} = \nu \cdot \frac{\partial^2 u}{\partial x^2} \tag{3}$$

has often been considered a natural one-dimensional model equation for turbulence

* This work was supported by ERDA under Grant AT-04-3-767.

ISSN 0021-9991

(see, for example, [21]). Equation (3) can be solved analytically and it is found that thin shocklike regions of width $O(\nu)$ separate smooth regions in long-term solutions. The purpose of the present work is to produce a series of flow pictures to investagete whether the 2-D equations also show any characteristic pattern in the solution.

Calculations similar to those presented here have been performed several times before using finite difference methods, e.g., [7, 12, 16, 17] or Fourier methods, e.g., [2, 9, 12]. After these original calculations the trend in more recent large-scale calculations has been to increase the spatial resolution rather than the integration time. In this paper the emphasis is the opposite. A new spectral filtering method is used in an attempt to provide a realistic model with a comparatively small mesh.

In some sequences of flow pictures we can follow the very organized physical structures which develop in the vorticity fields. These structures cast some doubt on the physical relevance of concepts like inertial range, energy spectrum, etc., which are based on the Fourier representation of the flow field. We study the energy spectrum mainly because extensive previous efforts have gone into theoretical predictions [13, 15, 22] and numerical estimates [7, 12, 16, 17] for it. The estimates for energy spectra presented here should not be considered as conclusive due to the limited resolution. However, they indicate that a power law for steady "turbulence," if any exists, probably is closer to k^{-4} than to k^{-3}.

Numerical Method

Equation (1), with the viscosity term left out, is approximated by the Fourier method. The viscosity is included in a separate step described below. The numerical properties of the Fourier (or pseudospectral) method, first developed by Kreiss and Oliger [14], have been analyzed for example in [8, 19]. The method has been applied to 2-D flow in a way much similar to the present work, by Orszag and others in [9, 12]. However the conclusions drawn by them differ strongly from those presented here. We believe that the present method is good enough to provide results relevant to flow structures and possibly to the form of the energy spectrum.

There are different ways to describe the idea of the Fourier method. One is to see it as a method to both obtain space derivatives of ω (the variable advanced in time by Eq. (1)) and to perform multiplications like $(\partial\psi/\partial x) \cdot (\partial\omega/\partial y)$, etc. all in spaces where the operations are local. With the use of the FFT algorithm, we can efficiently transform mesh functions such as the discretized ω from physical to Fourier space and back. In Fourier space, derivatives like $\partial\omega/\partial x$ and $\partial\omega/\partial y$ correspond to a single scalar multiplication of each mesh value and not to a convolution as in physical space. For physical products this situation is reversed and the factors are first brought to physical space before they are multiplied. In the present implementation new values of ψ at each time level together with its space derivatives, were also obtained by local operations in Fourier space. It is probable that the much faster method of using a fast Poisson solver, based on the five-point approximation of (2), together with numerical differentiation also would have been an adequate way to approximate the ψ-derivatives

in (1). After the evaluation of the right-hand side of (1) in the way described above, ω is brought to the next time level using leapfrog (central difference) time differencing.

The Fourier method gives approximations with very high formal order of accuracy. It is, nevertheless, surprising that this method is useful since truncated Fourier series representation of discontinuous or otherwise nonsmooth functions can be quite inaccurate (e.g. the Gibbs phenomenon), in particular if used to approximate derivatives at the mesh points. However, the method has been shown to be very accurate for long-time integrations even in such cases. This must mean that, with appropriate time differencing, the large oscillatory spatial errors have canceled to a high order. The influence of a nonsmooth variable coefficient is discussed in [8]. According to recent results [10], partially corrected leap-frog or Adams–Bashforth schemes may have a slight advantage over the conventional leap-frog scheme used here.

In [8, 14] the resolution power of this Fourier approach is compared with classical finite difference approximations for a linear problem. (There is no practical experience indicating any significant difference for nonlinear cases.) Leap-frog in time together with second- and fourth-order methods in space is shown to require typically 20 and 8 points, respectively per wavelength (the numbers depend on the desired accuracy, time interval, etc.) compared to 2 for the Fourier method. To obtain a certain final accuracy, the number of mesh points needed in each space dimension can be reduced in proportion to these numbers. Especially in problems with more than one space dimension, this leads to substantial savings in the computer time and high speed memory. Using classical finite difference methods, the problem described here would be beyond the capacity of all but possibly the very largest of presently existing computers.

The computations described in this paper were carried out on the IBM 370/158 computer at California Institute of Technology. Each time step for the 64×64-mesh required about 2 seconds of computer time (single precision arithmetic).

Treatment of the Viscosity Term

In a turbulent flow at large Reynolds number, the scales of the large eddies and the finest structures differ by several orders of magnitude. By inertial range is meant a range of intermediate scales in which the direct influence of viscosity is assumed to play only a minor role. On a a uniform rectangular mesh with the order of 100 points on a side, the largest and smallest scales that can be resolved differ by one order of magnitude at most The scaling and mesh size are assumed to be such that variations of the order of the mesh size (and smaller) are rapidly damped by viscosity Thus the smallest wavenumbers which viscosity damps rapidly must correspond to length scales quite close to the largest features represented on the mesh The variation of viscous decay with wavenumber is rather slow (cf formula (5) below) In these circumstances the interval of wavenumbers in Fourier space where viscosity is important covers the entire computational range and no inertial range can be detected. This seems to be the reason why it was concluded in [12] that simulation of the present

kind cannot be used to obtain information about an inertial range, unless the mesh is significantly refined. In the present study we introduce viscous decay that varies rapidly, indeed discontinuously, with wavenumber and thus are able to detect what could be described as an inertial range while only employing a 64×64 net.

In the calculations reported in [9, 12], the viscosity term was implemented by the use of an implicit difference scheme in physical space. It can also be implemented by repeated damping of the voriticity in Fourier space

$$\omega(x, y, t) = \sum_{k_1} \sum_{k_2} \hat{\omega}(k_1, k_2, t)\, e^{2\pi i(k_1 x + k_2 y)}. \tag{4}$$

A correct damping is obtained if $\hat{\omega}(k_1, k_2, t)$ is multiplied by

$$e^{-4\pi^2 \nu (k_1^2 + k_2^2)\Delta t} \tag{5}$$

at intervals Δt in time. For some of the calculations described below, this procedure has been used. With viscosity included in this way it is however very doubtful that one can observe an inertial range in calculations on a 64×64-mesh.

In this paper, we try to circumvent this problem by reexamining the way viscosity is applied. In the one-diemensional Eq. (3), a change in ν does not change the main flow picture, only the local steepness of the shock layer. In two dimensions, it was noticed in [9, 12] that the main flow picture was again very independent of the value of ν. It seems to be mainly in controlling the local steepness in thin structures that ν plays a role. It is then reasonable to ask if also the way it is applied might not affect the main structure, especially if the boundary of the region in which the viscosity acts can be made considerably sharper in Fourier space. This could leave an interval in Fourier space for an inertial range to develop. All wavenumbers higher than a certain limit are discarded (filtered) at regular intervals in time. Such elimination of high wavenumbers has been proposed before [20], but for a different purpose. Here it is used to model an energy sink rather than to eliminate "aliasing errors."

This idea of discarding high wavenumbers has some similarities in philosophy to subgrid modeling, which is being increasingly used. This technique is also based on a belief that the development of large scale structures do not essentially depend on the exact structure of the finest scales, but that a statistically correct model for these structures is sufficient.

In the present calculations, both "proper" viscosity (applied by damping of ω in Fourier space every 4 time steps) and sharp filtering (see below; elimination every 60 time steps of all modes with wavenumbers $\geqslant 20$) were used. Initial development of physical structures like stringy patterns and especially the large finite area vortex regions (FAVR) depend very little on this choice. The main difference is that with the second method, much less damping of energy and voritcity is needed in order to suppress the development of structures so small that their numerical resolution is in doubt. This reduced viscosity allows integration far beyond the time when otherwise fine structures would have been smoothed out.

An energy spectrum $E(k)$, $k = 0, 1, 2, \ldots$ can be introduced to express the total amount of kinetic energy in different frequency modes. For each value of k, a summa-

tion is made over all pairs of wavenumbers k_1, k_2 close to a radius k, say $k - \frac{1}{2} < (k_1^2 + k_2^2)^{1/2} < k + \frac{1}{2}$, in the Fourier representation of the velocity field. Some difficulties introduced by this definition are discussed in Appendix 1, where also an exact definition is given.

Numerical Results

Figures 1 to 15 show five series of flow pictures. For each flow situation which is illustrated, the top figure shows lines of constant vorticity and the bottom figure lines of constant streamfunction (i.e., streamlines). The lines for constant vorticity are continuous for negative values and dotted for positive values. To make the flow structures more visible, the difference in vorticity between the positive equilines is three times the difference between the negative equilines. The direction of the flow along the streamlines has been marked. In the beginning of series 1 the time interval between different figures is so small that the movement of individual features can be followed. In series 1 to 3 viscosity was implemented by setting to zero the amplitude of all frequency components with wavenumbers k greater than 20 (for two consecutive time levels to fit with the leap-frog time differencing) at every 60 time steps.

Series 1. Figures 1 to 7 and 17. The initial vorticity distribution was chosen to satisfy $E(0) = 0$, $E(k) = \text{constant}/k^3$ for $1 \leqslant k \leqslant 8$. $E(k) = 0$ for $k > 8$. (Some numerical values are given in Appendix 2.) All phases were randomly distributed in $[-\pi, \pi]$. The flow is seen to rapidly change structure to a stringlike vorticity pattern while developing towards two opposite directed FVAR. The maximum vorticity in one of them settled to a value about 50% bigger than the maximum value in the other. ($E(0)$ remained zero to within rounding error fluctuations.) Figure 17 shows selected energy spectra just after the filtering of wavenumbers has been performed.

Series 2. Figures 8 to 9 and 18 to 19. In the final state in series 1 (after 5220 time steps) all phases in the Fourier decomposition of ω were randomly redistributed in $[-\pi, \pi]$ without changing the magnitude of any component. Thus the energy spectrum remained unchanged. A development much the same as the one for series 1 is seen. This is discussed further below.

Series 3. Figures 10 to 13 and 20. The initial vorticity distribution satisfies $E(0) = 0$, $E(k) = \text{constant}/k$, $1 \leqslant k \leqslant 20$, $E(k) = 0$, $k > 20$. The phases are randomly distributed. This spectrum corresponds to an equidistribution of vorticity among the wavenumber pairs k_1, k_2 satisfying $0 < (k_1^2 + k_2^2)^{1/2} < 20.5$. Although the structures initially are much smaller than in series 1, the end state is similar with two opposite directed large-scale FAVR.

Other calculations performed (but not displayed by a sequence of flow pictures) included use of "proper" viscosity (series 4) and a test of the sensitivity of the solution to perturbations.

Normal viscosity (using $\nu((\partial^2\omega/\partial x^2) + (\partial^2\omega/\partial y^2))$ in Eq. (1)) was applied by damping

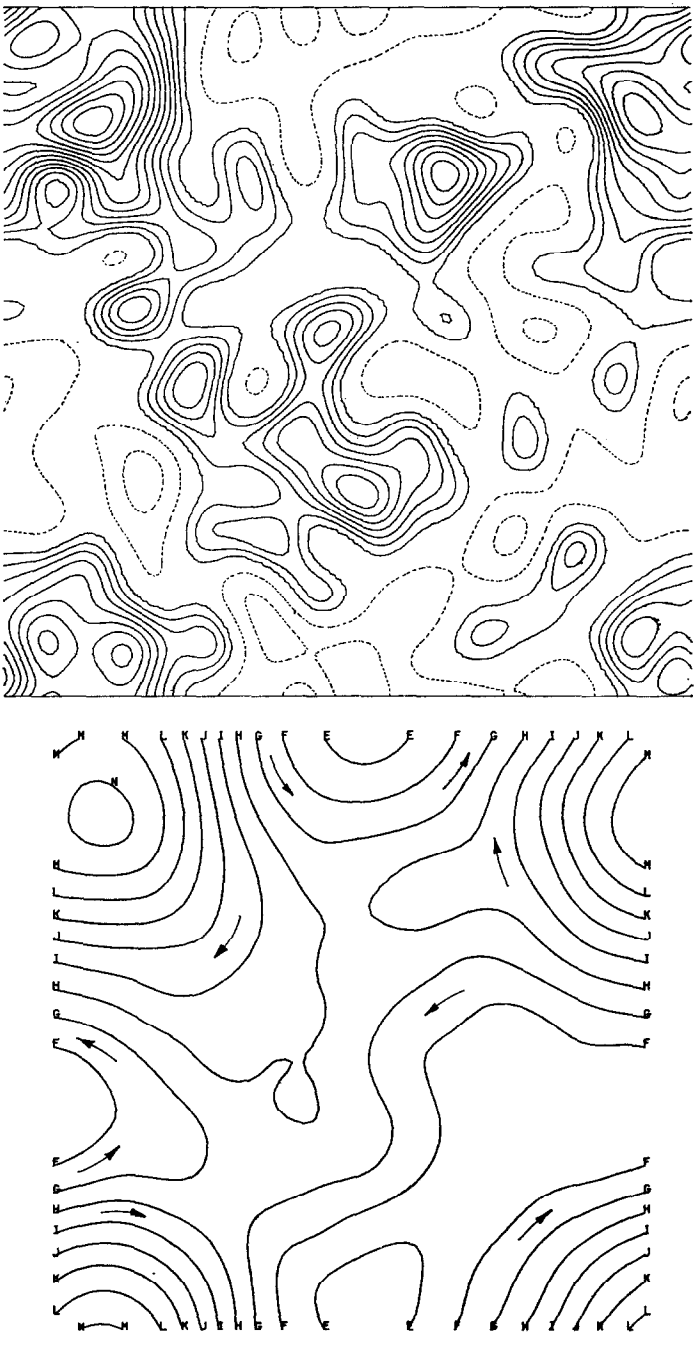

FIG. 1. 0 time steps; Series 1.

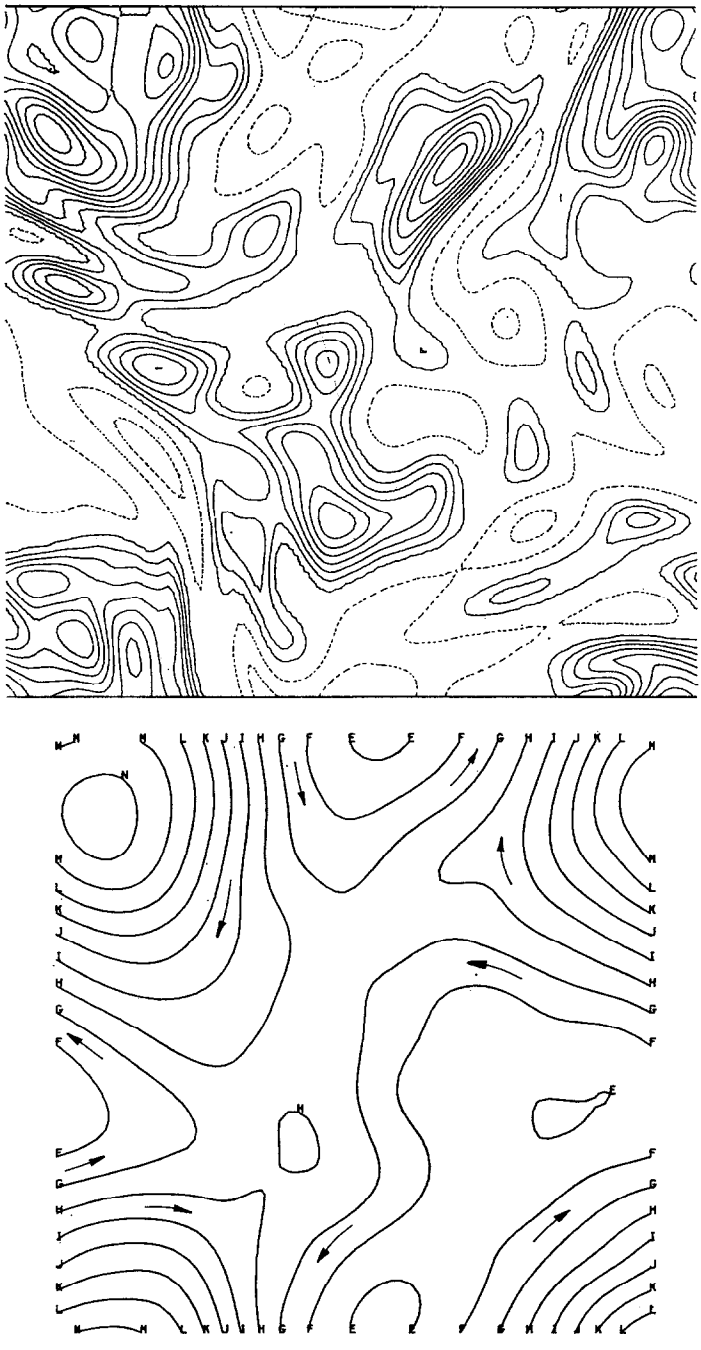

FIG. 2. 60 time steps. Series 1.

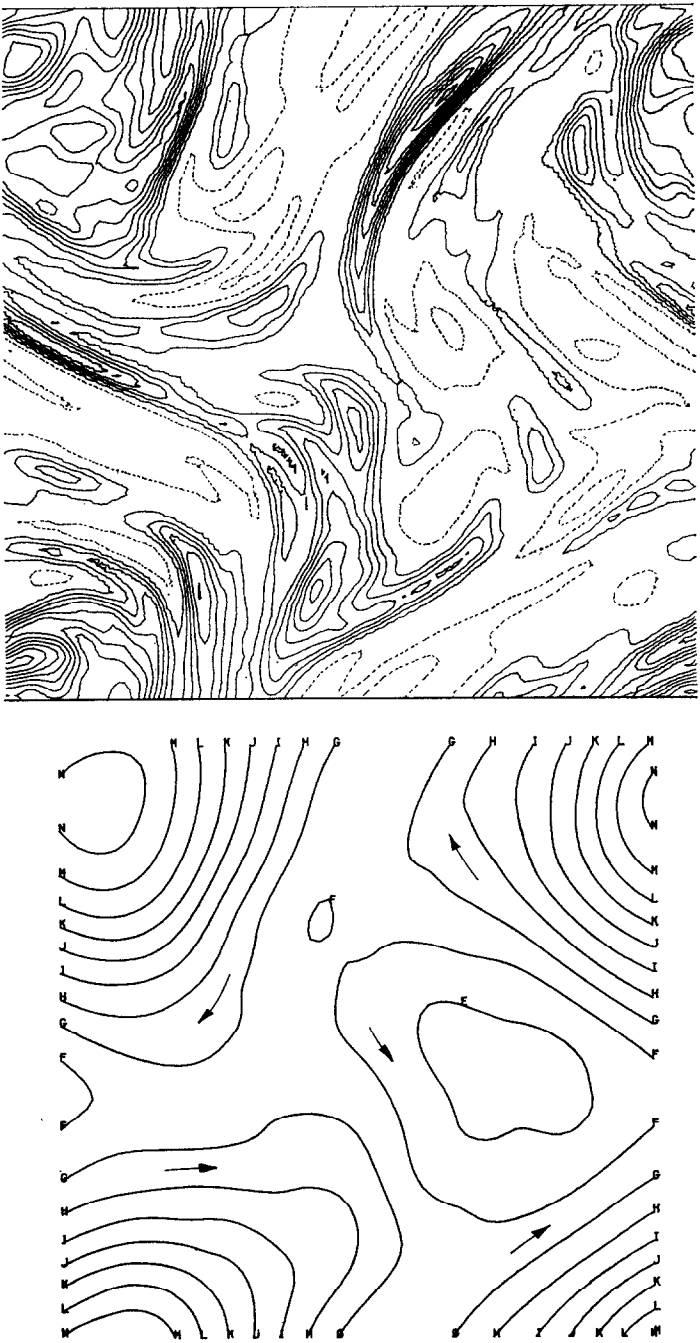

FIG. 3. 180 time steps; Series 1.

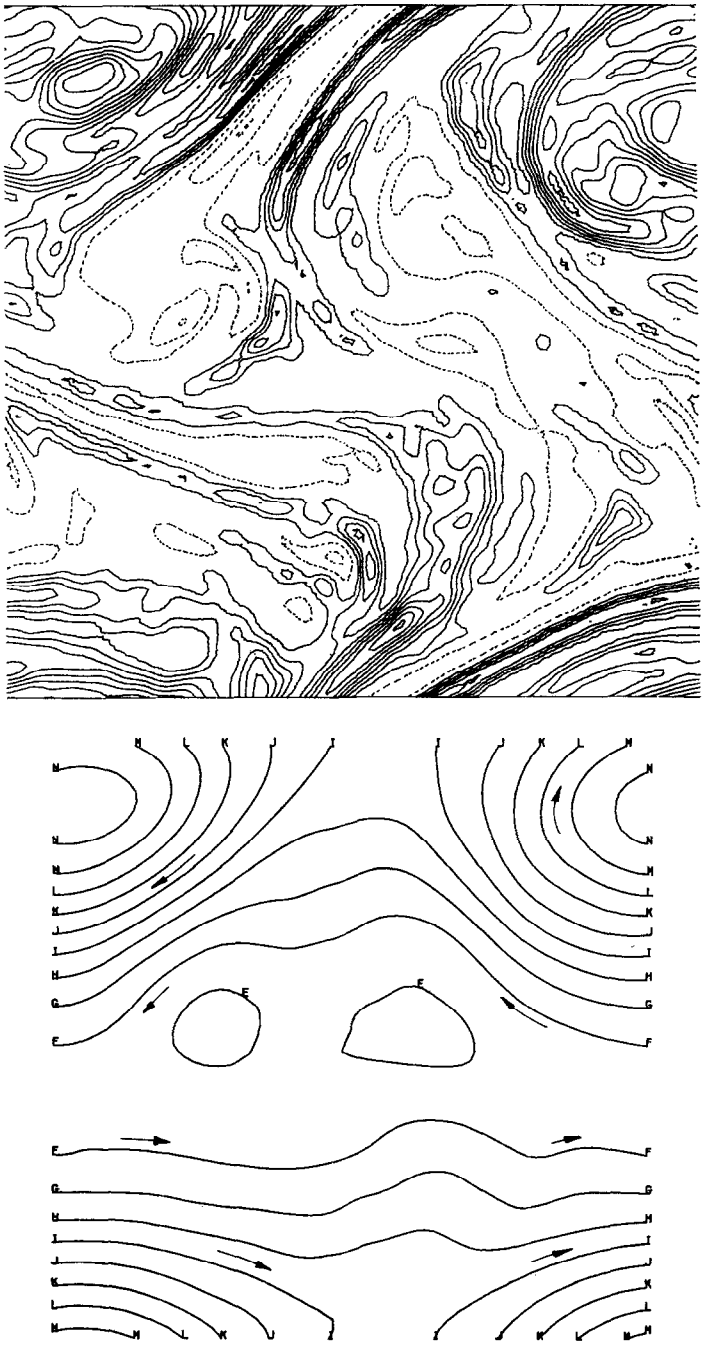

FIG. 4. 360 time steps; Series 1.

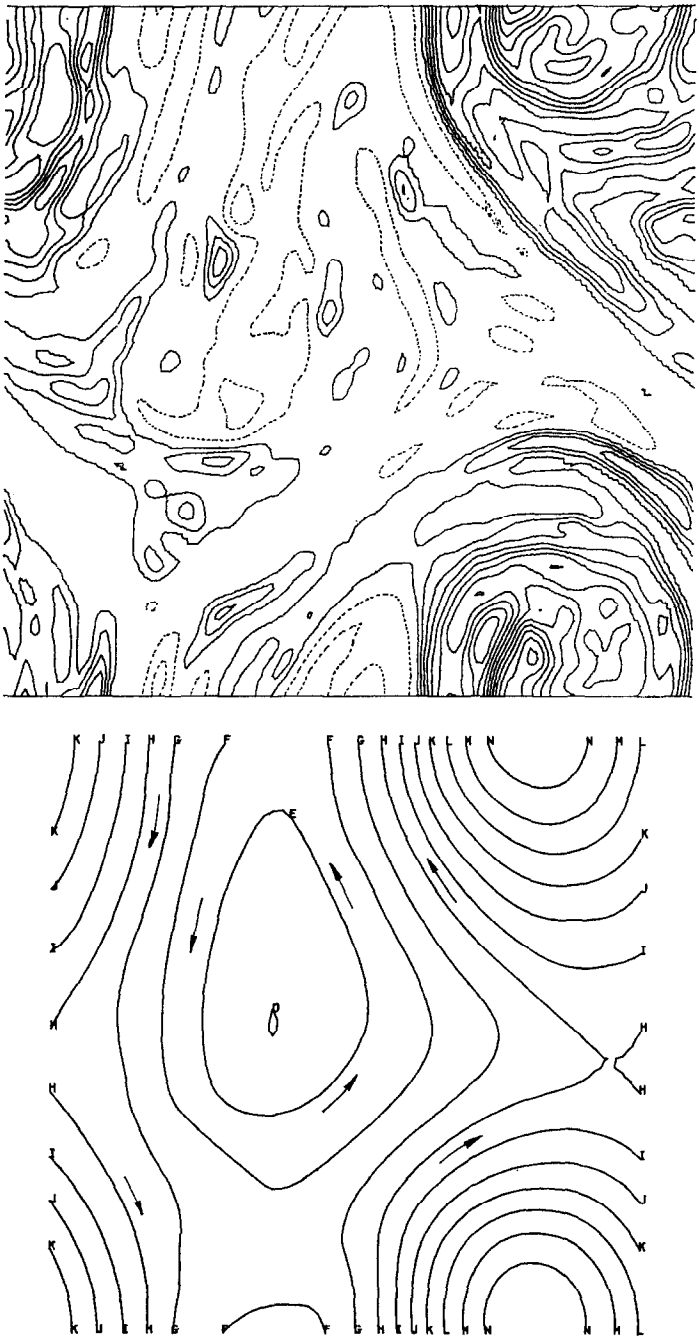

FIG. 5. 900 time steps; Series 1.

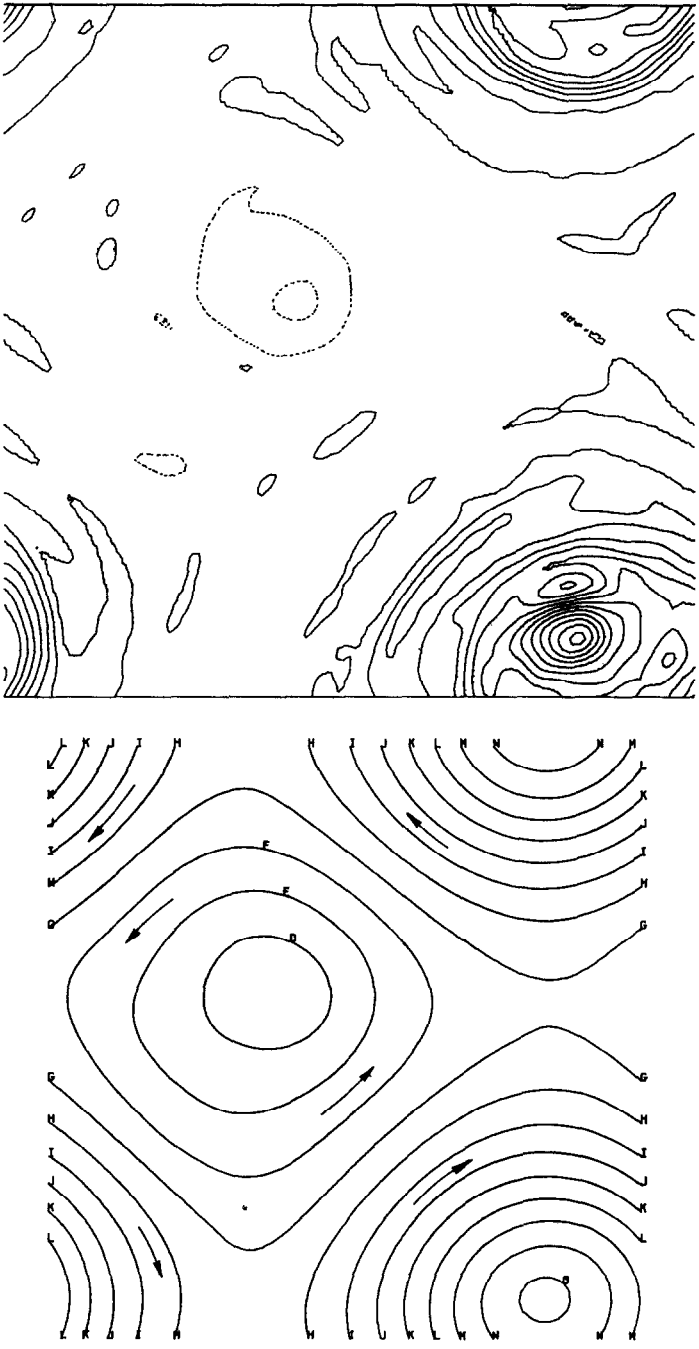

FIG. 6. 3060 time steps; Series 1.

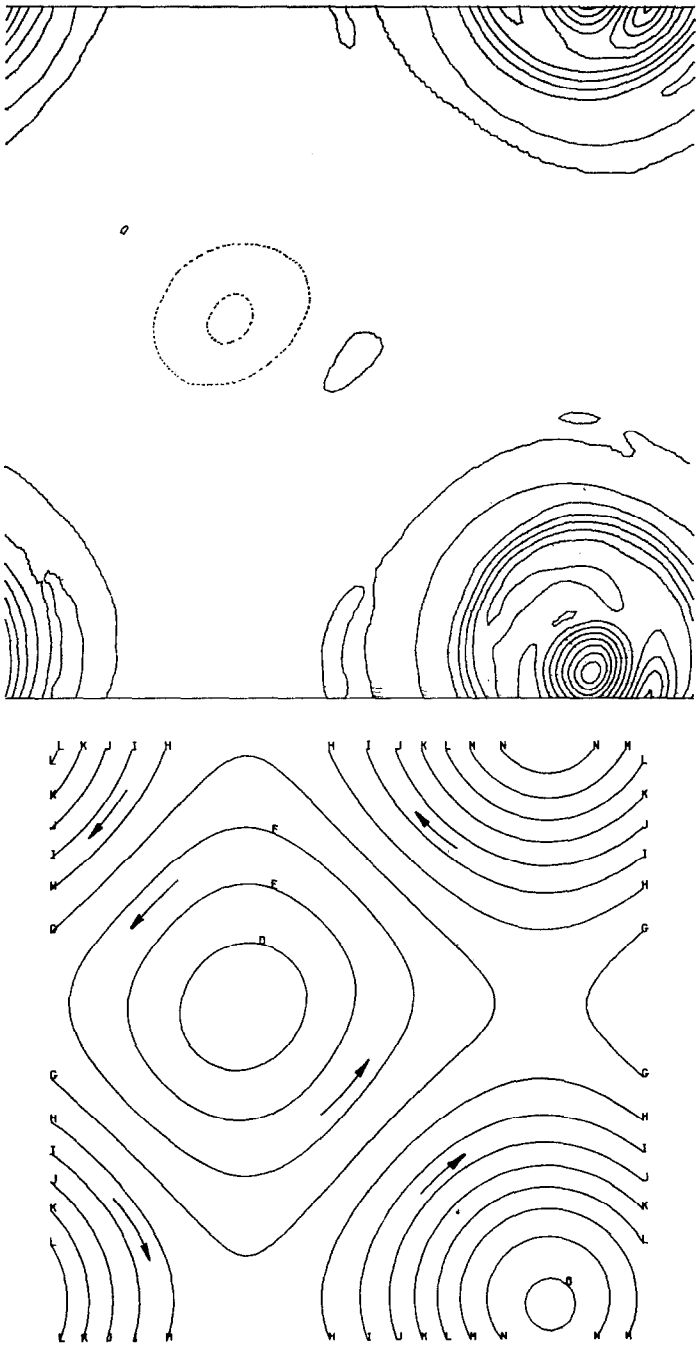

FIG. 7. 5220 time steps; Series 1.

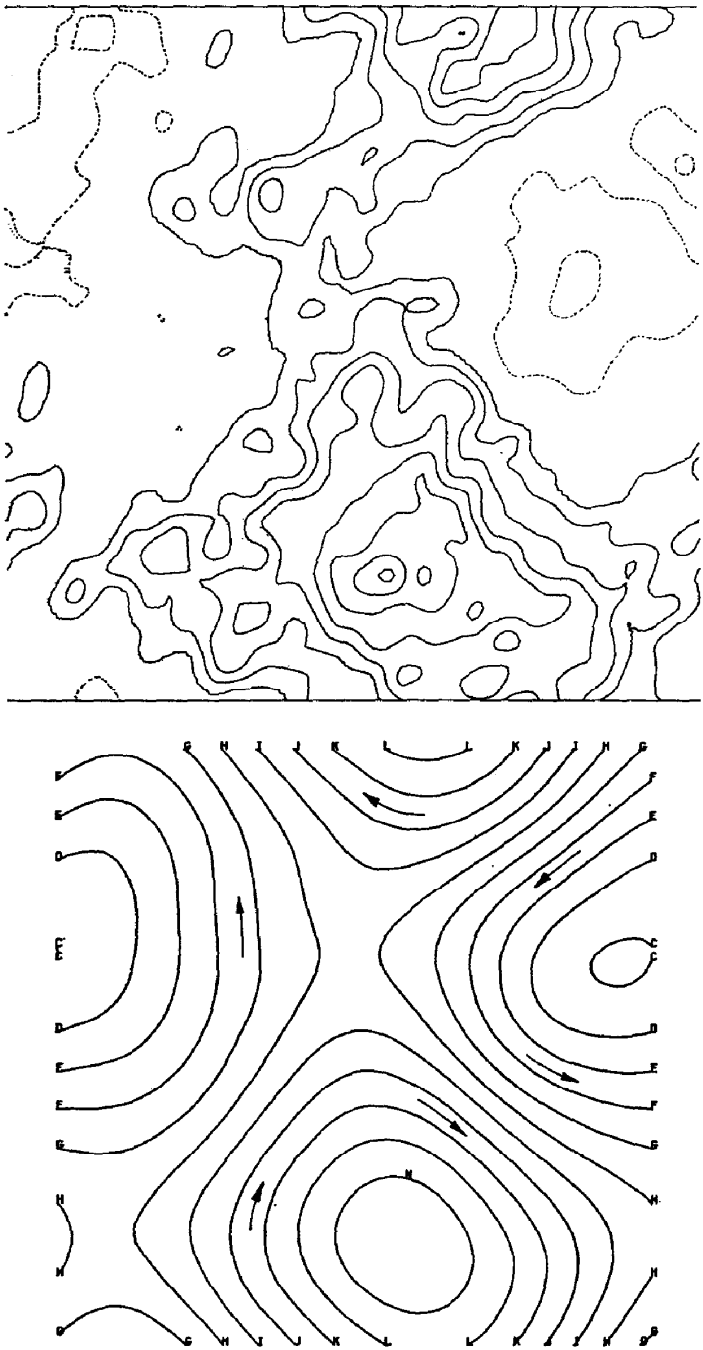

FIG. 8. 0 time steps; Series 2.

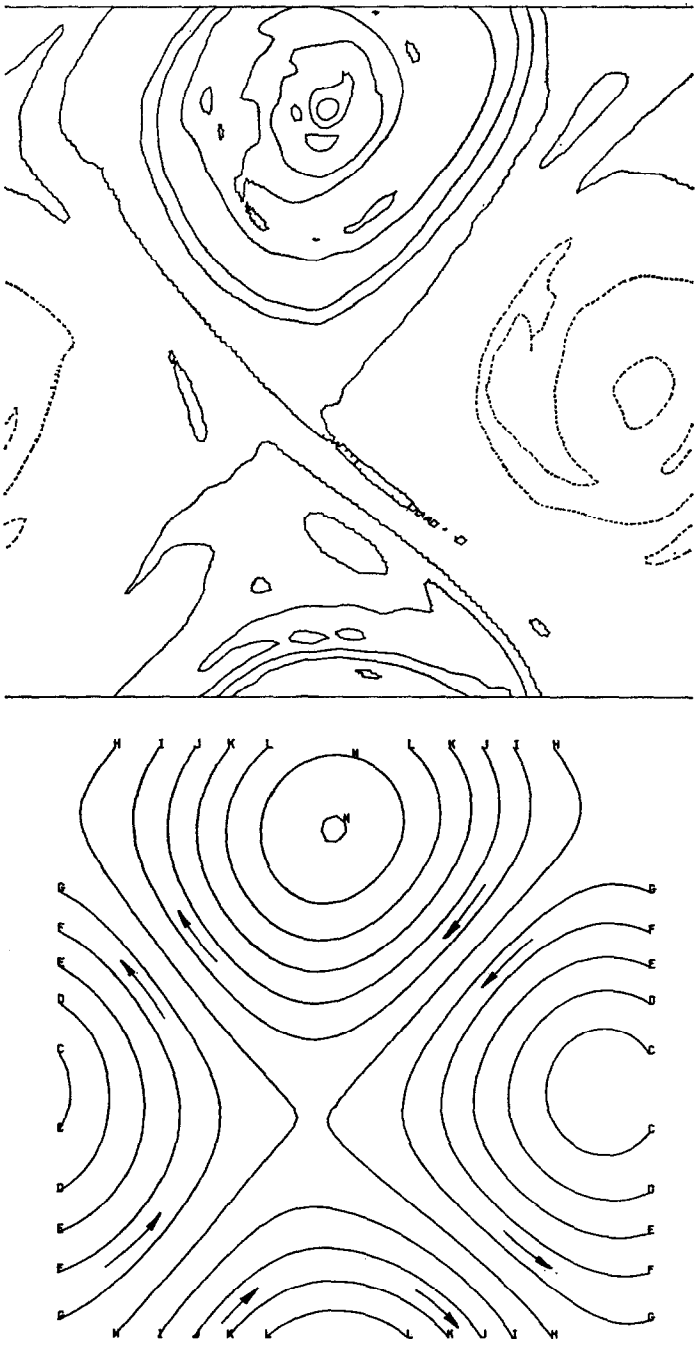

FIG. 9. 3060 time steps; Series 2.

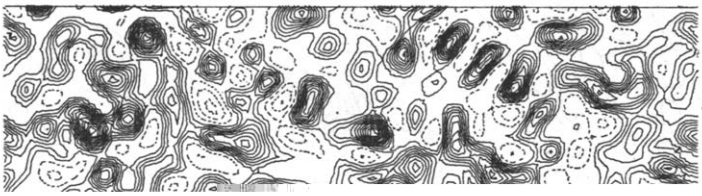

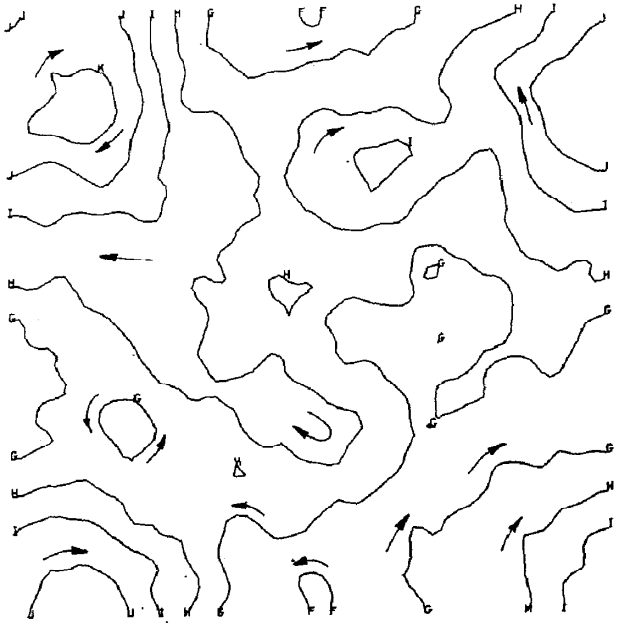

FIG. 10. 0 time steps; Series 3.

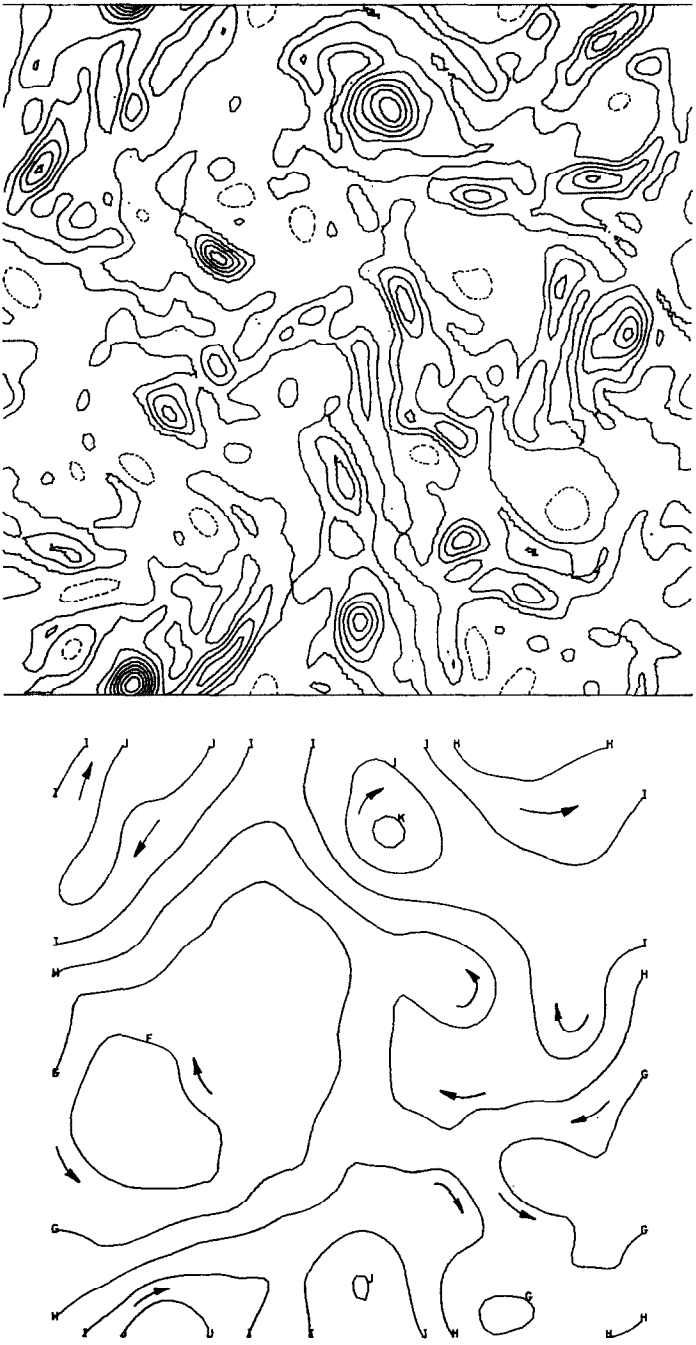

FIG. 11. 540 time steps; Series 3.

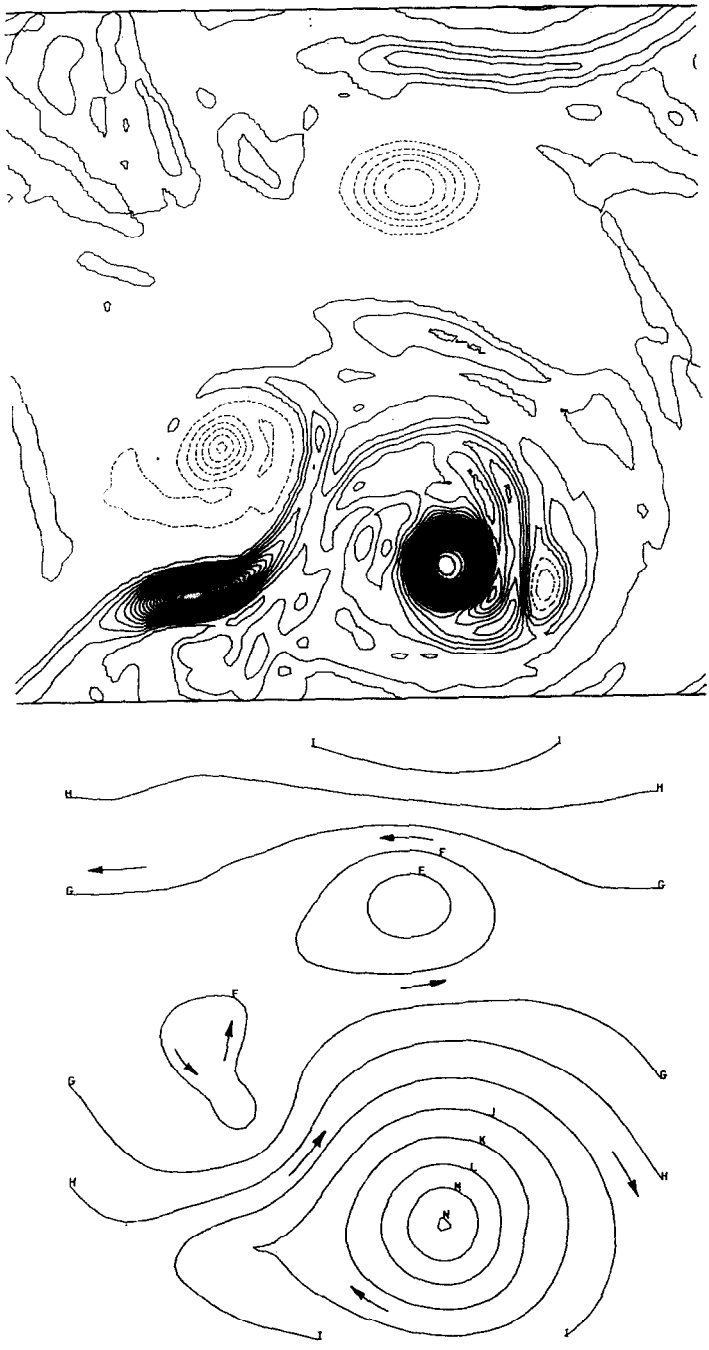

FIG. 12. 4320 time steps; Series 3.

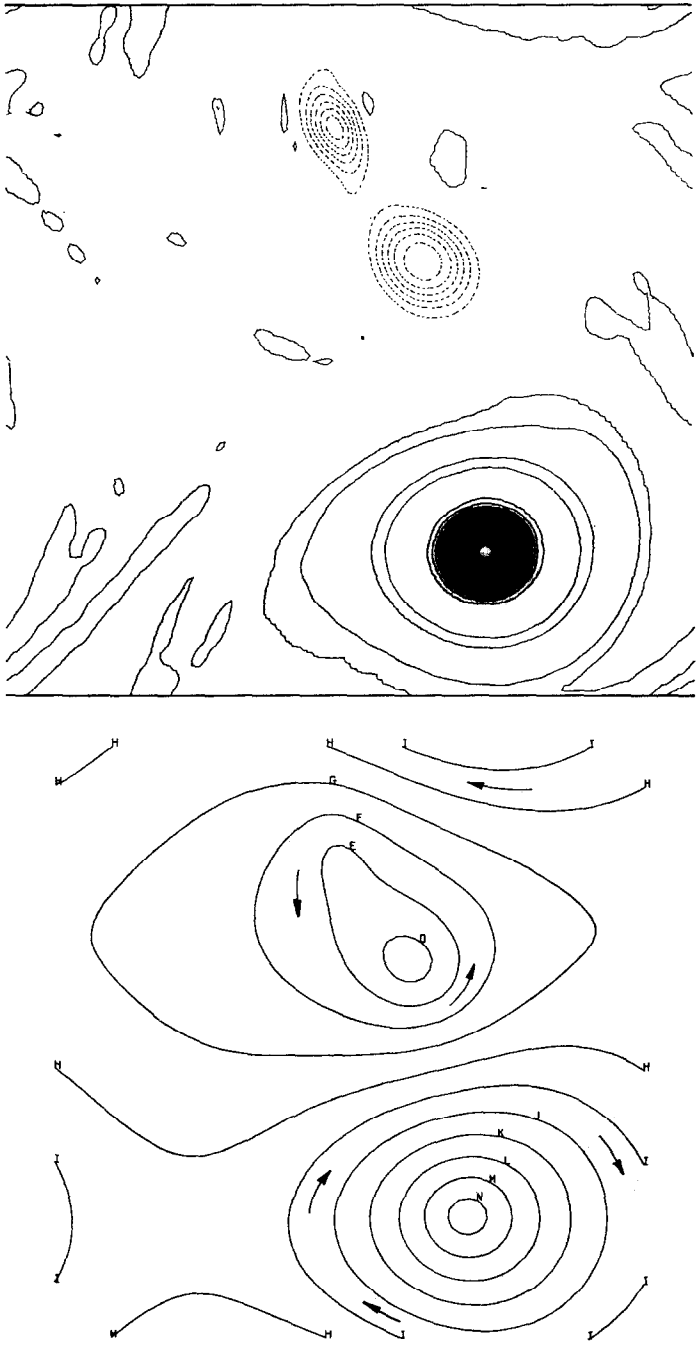

FIG. 13. 7020 time steps; Series 3.

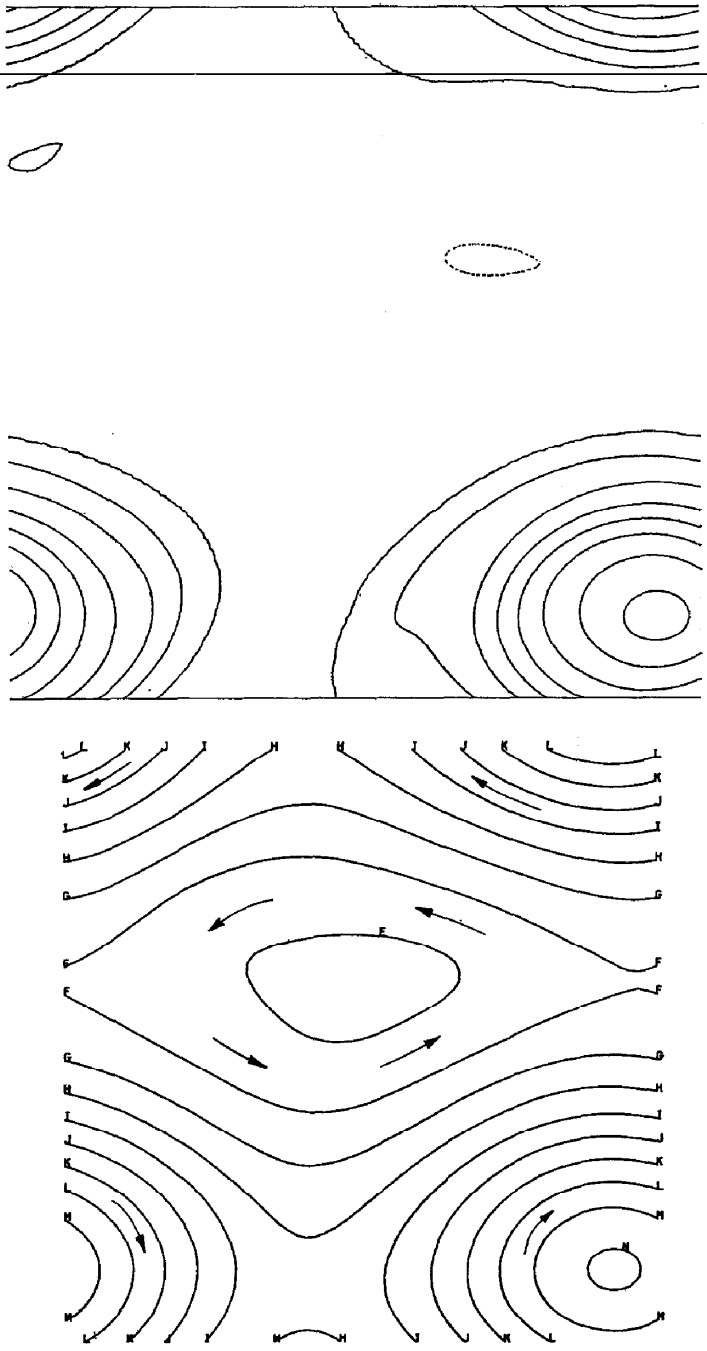

FIG. 14. 1980 time steps; Series 4.

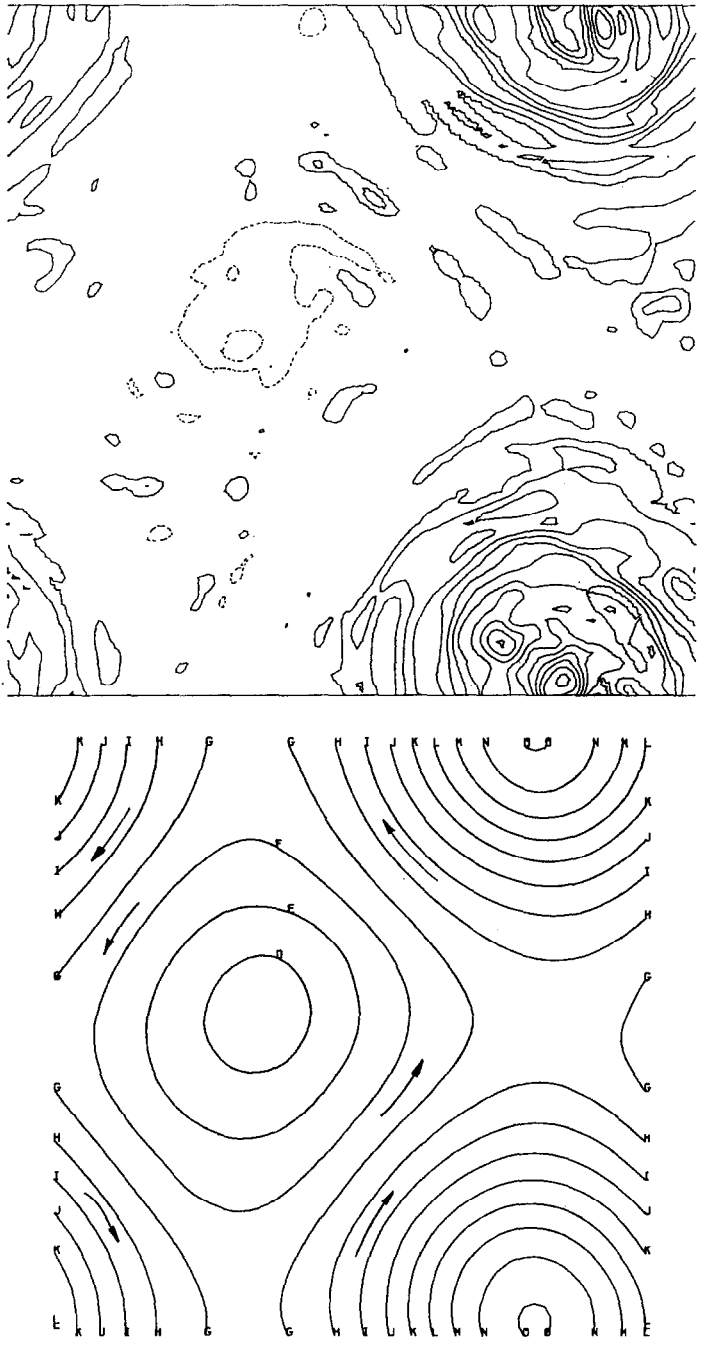

FIG. 15. 3060 time steps; Series 5.

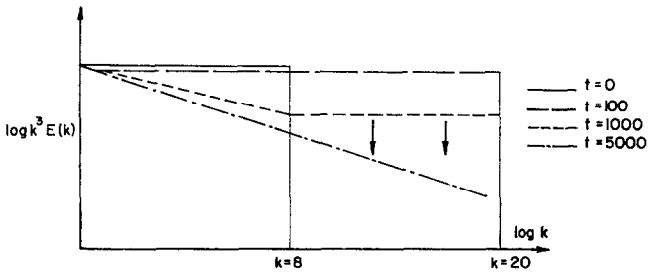

FIG. 16. Schematic development of energy spectrum.

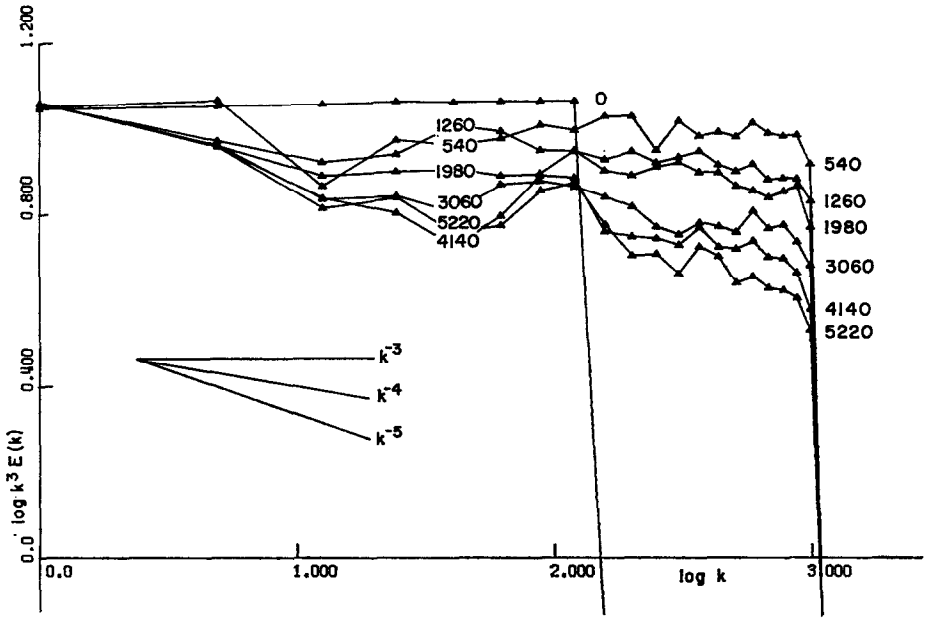

FIG. 17. Energy spectra in series 1.

of the Fourier coefficients for the vorticity (on the last two time levels) every four time steps. The $4\pi^2\nu\Delta t$ in formula (5) was 0.00015 (see Appendix 2 for an interpretation of this number). This value was found to be the lowest value possible that prevented structures from becoming too small for the mesh to resolve. This dissipation acts over a wide range of frequency components, including the low ones, which contain large amounts of energy. In these runs, the flow again rapidly developed to two FAVR but with less fine structure and with an energy spectrum decaying more rapidly than k^{-4}, especially for high wavenumbers. This probably indicates that the whole calculation was within the viscous range and that there was nothing which possibly could be described as an inertial range.

A test was performed (using the sharp filtering method) with small scales structures superposed on the initial state of series 1. Even fine structures in later flow pictures

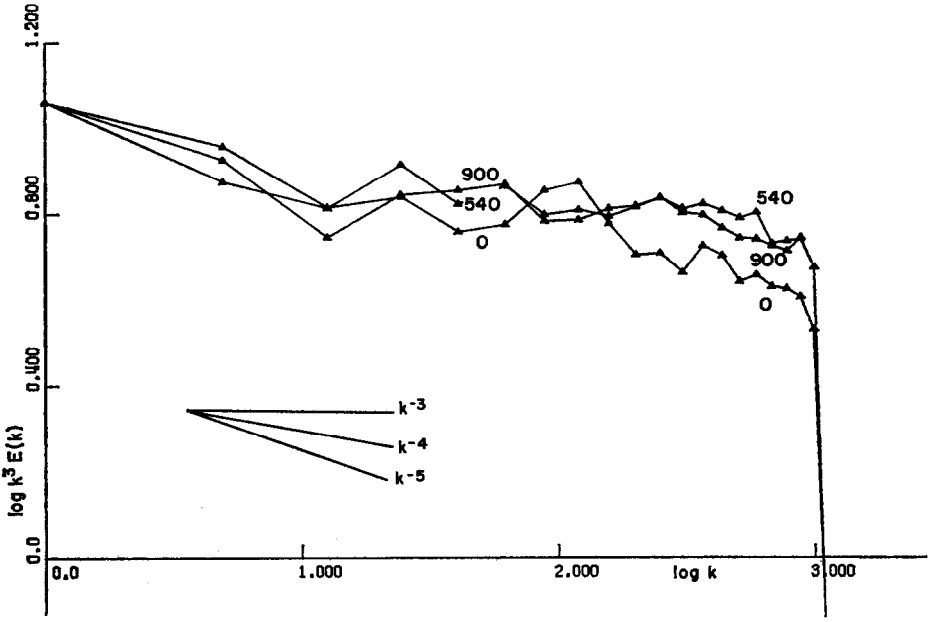

FIG. 18. Energy spectra in series 2; continued in Fig. 19.

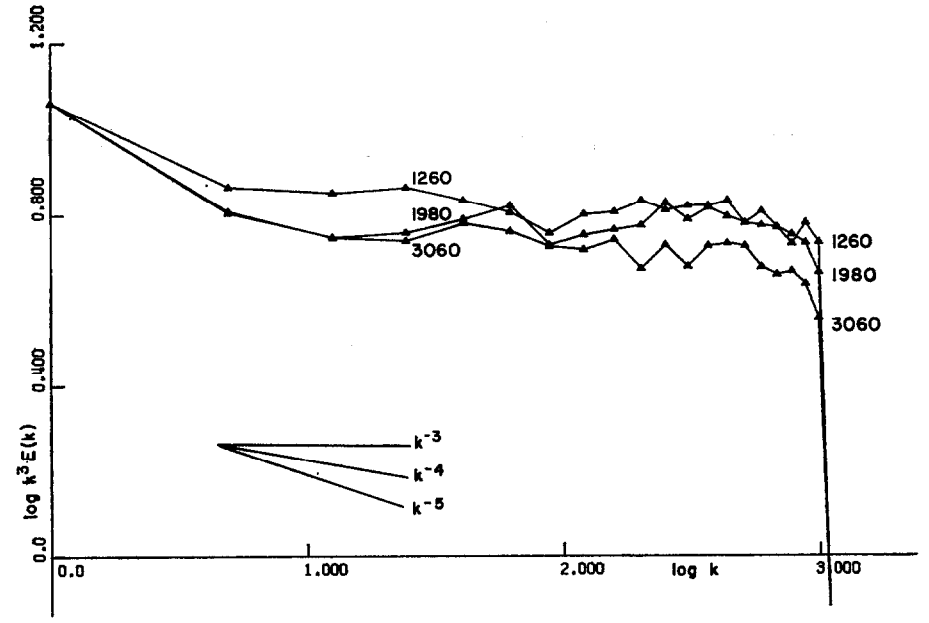

FIG. 19. Energy spectra in series 2. continuation from Fig. 18.

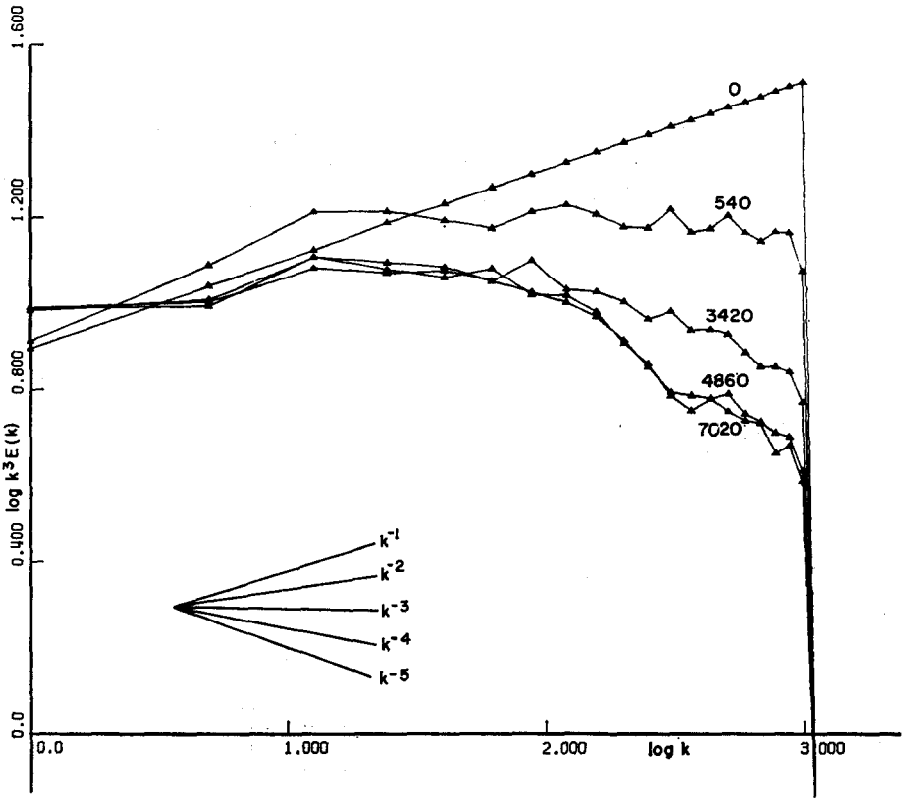

FIG. 20. Energy spectra in series 3.

remained virtually unchanged between the two runs. This indicates that the 2-D Navier–Stokes equations form a well-conditioned problem with respect to small-scale perturbations.

A further series of calculations were carried out for a case with an initial spectrum $E(k) = 0$, $k = 1, 2$, $E(k) = \text{constant}/k^2$ for $3 \leqslant k \leqslant 20$ and $E(k) = 0$, $k > 20$ (sharp filtering method). The energy in wavenumber one, which is dominant in a state with two FAVR was initially zero. The purpose was to see if a state with more than two FAVR would be reached. However the flow development followed closely the one in series 3. The different zones of positive and negative vorticity which first appeared gradually joined up to form two FAVR.

The time development of the total energy and enstrophy (mean square vorticity) in series 1 to 4 is shown in Figs. 22 and 23. (The units on the vertical axis in each figure are the same for the four curves but otherwise arbitrary.)

Cascade arguments for 3-D turbulence predict that both energy and enstrophy flow from low to high wavenumbers. In 2-D turbulence most energy is dissipated at low wavenumbers and, if a cascade argument is still relevant, it would imply that energy and enstrophy flow in opposite directions. Figures 22 and 23 seem to be consistent

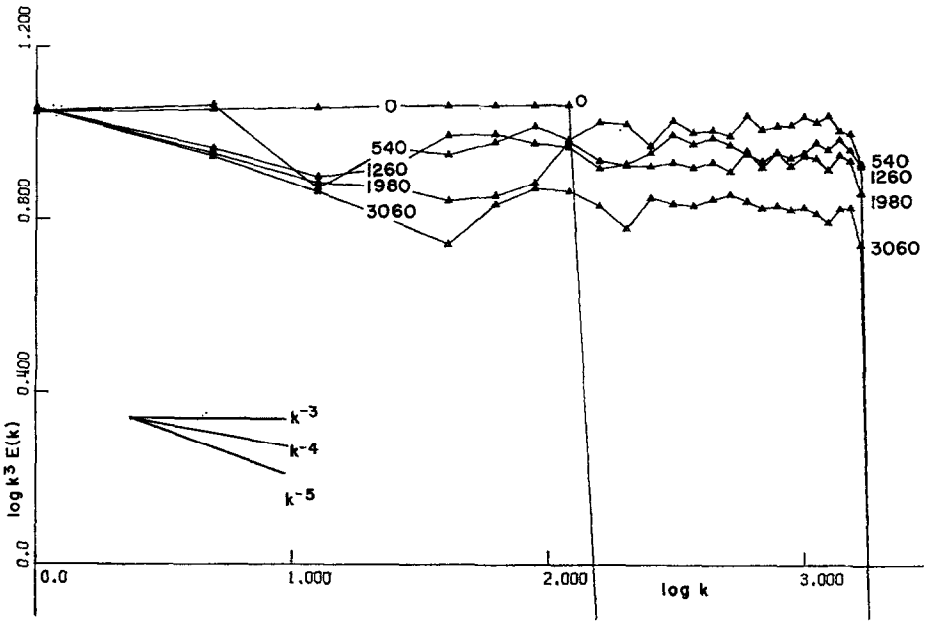

FIG. 21. Energy spectra in series 5.

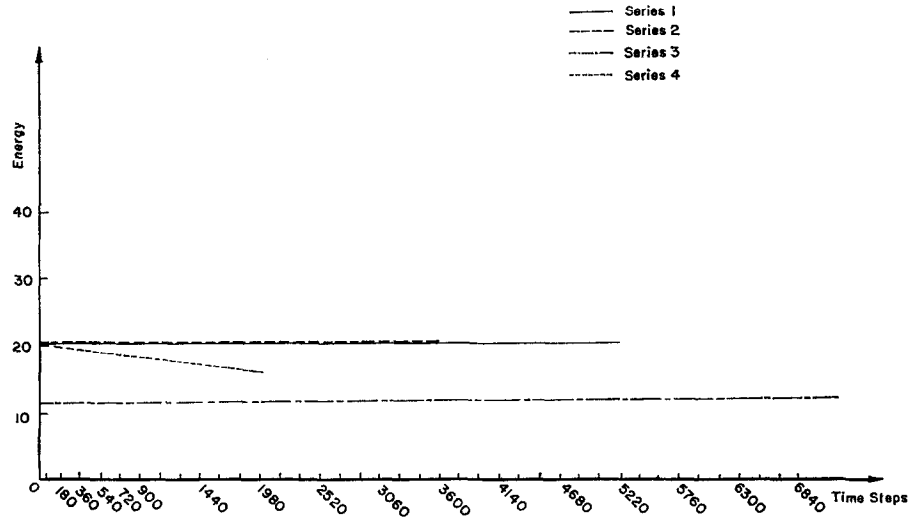

FIG. 22. Total energy as function of time.

with this description. In all cases the original energy and enstrophy were confined to the first 20 wavenumbers. The time independence of the total energy using the sharp filtering method corresponds to the fact that no energy penetrated towards higher wavenumbers. The enstrophy, on the other hand, is decaying in all cases.

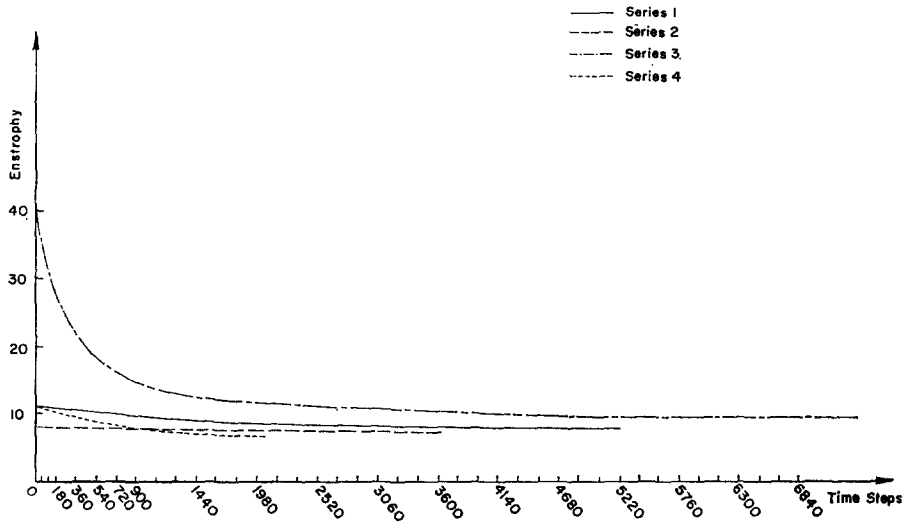

FIG. 23. Total enstrophy as function of time.

Ideally we would wish to use infinitely many wavenumbers and "proper" viscosity with coefficient ν decreasing to zero. As discussed above this is not possible to achieve with the use of a finite grid allowing only a very limited resolution. What a model for subgrid structures should achieve is to make the components for low wavenumbers develop as if the higher ones were present and correctly treated. The conservation of the total energy in the lowest 20 wavenumbers is therefore in agreement with the physical problem. (The numerical scheme in itself is not energy conserving. The conservation can be seen as a test of accuracy.) With the use of "proper" viscosity, a strong decay of energy seems to be inevitable.

The sharp filtering method contains two parameters k_{cut} and n_1. They describe at which wavenumber the cutoff was performed and how often it was done. One more parameter enters because of a special property of leap-frog time differencing. The solution at every second time step may separate from the other time steps. This effect can be suppressed by coupling the scheme together at every n_2 time steps. (We can, for example, introduce time levels $t + k/2$ and $t + (3k/2)$ as the average of levels t, $t + k$, and $t + k$, $t + 2k$, respectively. The scheme can be restarted from the two new levels.) In series 1 to 3 we used $k_{\text{cut}} = 20$, $n_1 = 60$, and $n_2 = 60$. It is crucial for our model of the energy sink that changes in these numbers do not significantly change any flow characteristics. In separate test runs all the three parameters were varied both individually and together to test their possible influence on the solution. Changing k_{cut} from 20 to 25 only extended the spectrum to five more wavenumbers. Components just before the original cutoff, i.e., say 18 and 19 did not virtually change at all. The time interval between these filterings, n_1, was changed from 60 to 6. In contrast to what one might guess at first, this slightly increased the amounts of high frequency components. Otherwise the nature of the spectrum did not change. Finally

n_2 was changed from 60 to 30 with no noticable effect. This indicates that the separation of every second time level was satisfactorily suppressed already using $n_2 = 60$. Figures 15 and 21 (series 5) show a repetition of the run in series 1 up to time level 3060 with $k_{\text{cut}} = 25$, $n_1 = 6$, and $n_2 = 30$ (instead of $k_{\text{cut}} = 20$, $n_1 = n_2 = 60$). The flow Fig. 15 show little difference to Fig. 6 and the corresponding spectra, slightly higher for higher wavenumbers, again agree very well with the schematical description in Fig. 16.

Conclusions

The development of the spectrum in series 1 can be illustrated schematically as shown in Fig. 16. During the initial stages, before the phases have had time to reach natural correlations, we find that the energy spectrum fairly rapidly adapts to a third power law. However, as FAVR and phase correlations develop, it seems to approach something closer to a fourth power law. The development of FAVR in two-dimensional flow was predicted from different approaches by Onsager [18] and Batchelor [1]. Saffman [22] showed that such a structure would lead to a k^{-4} spectrum if the boundaries between the FAVR had steep vorticity gradients. However, the flow pictures in the present calculations do not seem to confirm this assumption. Energy spectra decaying faster than k^{-3} have actually been obtained numerically several times but it appears that most authors have discarded such results as due to various forms of errors since they did not agree with the expected result. However in[7] convergence to a fourth power law is reported.

Series 2 serves to test the influence of phase correlations. All correlations in the final state in series 1 were destroyed by randomizing all phases but keeping all magnitudes the same. Without the proper phase correlations, an "unnatural" burst of high frequency components gets initially generated. This brings the spectrum from fourth to third power during the first 500 to 1000 time steps. After that the development in series 1 (and convergence to fourth power) seems to be repeated.

This experiment illustrates one difficulty in the theoretical study of turbulence by arguments based only on magnitudes of Fourier components.

The development in series 3 can be compared to the results on inviscid flow reported by Seyler *et al.* in [23]. They consider the plane nonviscous Navier–Stokes equations in a Fourier space truncated to a finite number of wavenumbers. The equilibrium arguments of statistical mechanics, for a system with a finite number of degrees of freedom, predicts for this case an energy spectrum.

$$E(k) \sim k/(\alpha + \beta k^2). \tag{6}$$

Here, α and β are constants which can be determined from the mean square energy and vorticity (both conserved). Numerical results in [23] show good agreement with (6). The initial state in series 3 fits (6) with $\alpha = 0$. Nevertheless, the solution deviates immediately from this distribution to follow the patterns discussed above for series 1

and 2. It would seem that a nonvisous formulation with a finite number of degrees of freedom describes a process fundamentally different from two-dimensional turbulence.

The cores of vorticity in series 3 might be somewhat sharper than they would have been with the use of normal viscosity. A calculation with higher resolution could be the best way to settle this question.

Appendix

1. *Definition of Energy Spectrum*

Transforming ω to Fourier space gives a 64×64 array of Fourier coefficients with wavenumbers up to 32 in each space direction

$$\omega(x, y) = \sum_{k_1} \sum_{k_2} \hat{\omega}(k_1, k_2)\, e^{2\pi i(k_1 x + k_2 y)} \qquad |k_1|, |k_2| \leqslant 32. \tag{7}$$

The total kinetic energy E can be evaluated as

$$E = \tfrac{1}{2} \sum_{k_1} \sum_{k_2} |\hat{\omega}|^2/(k')^2 \tag{8}$$

where $(k')^2 = k_1^2 + k_2^2$.

The most natural way to define an energy spectrum $E(k)$, $k = 0, 1, 2, \ldots$ would seem to be

$$E(k) = \tfrac{1}{2} \sum_{|k'-k| \leqslant \frac{1}{2}} |\hat{\omega}|^2/(k')^2 \tag{9}$$

satisfying

$$E = \sum_{k=0}^{\infty} E(k). \tag{10}$$

The double sum in (8) has in (10) been reordered into summation over circular rings around the origin. The number of integral lattice points in these different circular rings, i.e., the number of terms in (9), approach asymptotically $2\pi k$, but the number fluctuates considerably and seemingly randomly for small values of k. Even if $\hat{\omega}$ is a smooth function of k_1 and k_2, this will make $E(k)$ fluctuate irregularly.[1] Since $E(k)$ is used for graphic illustrations,[2] it was instead defined as the average value of $\pi |\hat{\omega}|^2/k'$ over all k' such that $|k' - k| \leqslant \frac{1}{2}$.

[1] The fluctuations this effect causes appear to be correlated to the fluctuations in the energy spectra in [12].

[2] The $E(k)$ displayed in Figs. 17 to 21 differ from this definition by a constant factor, i.e., to a translation in the log–log diagrams.

2. *Time and Space Units, Magnitude of Solution*

The periodic region in space was assumed to be a unit square. The numerical space step was 1/64 and the time step was 1/10 in all the calculations (i.e., the leap-frog time differences used values 1/5 time unit apart at each time step). Since the equations are nonlinear, the time unit is connected to the magnitude of the solution. (If ω and ψ are multiplied by a scalar, they will again satisfy (1) and (2) if we adjust ν and the time unit.) The equilines for the streamfunction in Figs. 1 to 15 differ by 0.001. They differ by 0.05 for negative vorticity and 0.15 for positive vorticity with the exception of Figs. 10 and 11 where the differences are four times larger. The zero equiline is marked with the letter H for the streamfunction. The value 0.00015 for $4\pi^2\nu\Delta t$ in the runs with "proper" viscosity corresponds to $\nu \simeq 10^{-5}$ ($\Delta t = 0.4$) since the viscosity was applied every four time steps.

3. *Implementation of the Fast Fourier Transforms*

The Fast Fourier transform algorithm (FFT) [3, 4, 6] has found wide-spread use in a large number of fields during the last ten years. It is described most naturally for the case of complex transforms. When general real transforms or real symmetric and antisymmetric transforms are needed, complex transforms over half or a quarter of the number of points can be used in connection with some simple additional algorithms [5]. With the use of such techniques, the only transform needed for the present work was a transform over 16 complex points.

In most descriptions of the FFT algorithm, an operation count of $C_1 N \log N$ is quoted (N is the number of points; the constant C_1 depends on what is counted). Comparisons with classical algorithms, $C_2 \cdot N^2$, turn out very advantageous if N is large. The potential of FFT for N small is seldom fully recognized and not well described by the asymptotic formula for N large. For this reason, the present implementation is briefly described. It is related but not identical to the usual implementations for N large.

We write the linear transform from Fourier to physical space.

$$\begin{bmatrix} X(0) \\ X(1) \\ X(2) \\ X(3) \\ \vdots \\ X(15) \end{bmatrix} = 1/N^{1/2} \begin{bmatrix} w^0 & w^0 & w & w^0 & \cdots & w^0 \\ w^0 & w^1 & w^2 & w^3 & \cdots & w^{15} \\ w^0 & w^2 & w^4 & w^6 & \cdots & w^{30} \\ w^0 & w^3 & w^6 & w^9 & \cdots & w^{45} \\ \vdots & & & & & \\ w^0 & w^{15} & w^{30} & w^{45} & \cdots & w^{225} \end{bmatrix} \begin{bmatrix} A(0) \\ A(1) \\ A(2) \\ A(3) \\ \vdots \\ A(15) \end{bmatrix} \tag{11}$$

where $w = e^{2\pi i/16}$.

We want to perform the matrix times vector multiplication in (11) as fast as possible. One way to understand the Fast Fourier transform method is to note that the matrix can be factorized into a product of sparse matrices. One of several systematic approaches is given in [11]. The factorization we have used for the matrix in Eq. (11) is $W_{16} = F_1 \cdot F_2 \cdot F_3$ where

$$F_1 = \left[\begin{array}{cccc|cccc|cccc|cccc} 1 & 1 & 1 & 1 & & & & & & & & & & & & \\ & & & & 1 & 1 & 1 & 1 & & & & & & & & \\ & & & & & & & & 1 & 1 & 1 & 1 & & & & \\ & & & & & & & & & & & & 1 & 1 & 1 & 1 \\ \hline 1 & i & -1 & - & & & & & & & & & & & & \\ & & & & 1 & i & -1 & -i & & & & & & & & \\ & & & & & & & & 1 & i & -1 & -i & & & & \\ & & & & & & & & & & & & 1 & i & -1 & -i \\ \hline 1 & -1 & 1 & -1 & & & & & & & & & & & & \\ & & & & 1 & -1 & 1 & -1 & & & & & & & & \\ & & & & & & & & 1 & -1 & 1 & -1 & & & & \\ & & & & & & & & & & & & 1 & -1 & 1 & -1 \\ \hline 1 & -i & -1 & i & & & & & & & & & & & & \\ & & & & 1 & -i & -1 & i & & & & & & & & \\ & & & & & & & & 1 & -i & -1 & i & & & & \\ & & & & & & & & & & & & 1 & -i & -1 & i \end{array}\right], \tag{12}$$

$$F_2 = \left[\begin{array}{cccc|cccc|cccc|cccc} 1 & & & & & & & & & & & & & & & \\ & 1 & & & & & & & & & & & & & & \\ & & 1 & 1 & & & & & & & & & & & & \\ \hline & & & & 1 & & & & & & & & & & & \\ & & & & & w & & & & & & & & & & \\ & & & & & & w^2 & & & & & & & & & \\ & & & & & & & w^3 & & & & & & & & \\ \hline & & & & & & & & 1 & & & & & & & \\ & & & & & & & & & w^2 & & & & & & \\ & & & & & & & & & & i & & & & & \\ & & & & & & & & & & & w^6 & & & & \\ \hline & & & & & & & & & & & & 1 & & & \\ & & & & & & & & & & & & & w^3 & & \\ & & & & & & & & & & & & & & w^6 & \\ & & & & & & & & & & & & & & & w^9 \end{array}\right], \tag{13}$$

$$F_3 = \left[\begin{array}{cccc|cccc|cccc|cccc}
1 & & & & 1 & & & & 1 & & & & 1 & & & \\
 & 1 & & & & 1 & & & & 1 & & & & 1 & & \\
 & & 1 & & & & 1 & & & & 1 & & & & 1 & \\
 & & & 1 & & & & 1 & & & & 1 & & & & 1 \\
\hline
1 & & & & i & & & & -1 & & & & -i & & & \\
 & 1 & & & & i & & & & -1 & & & & -i & & \\
 & & 1 & & & & i & & & & -1 & & & & -i & \\
 & & & 1 & & & & i & & & & -1 & & & & -i \\
\hline
1 & & & & -1 & & & & 1 & & & & -1 & & & \\
 & 1 & & & & -1 & & & & 1 & & & & -1 & & \\
 & & 1 & & & & -1 & & & & 1 & & & & -1 & \\
 & & & 1 & & & & -1 & & & & 1 & & & & -1 \\
\hline
1 & & & & -i & & & & -1 & & & & i & & & \\
 & 1 & & & & -i & & & & -1 & & & & i & & \\
 & & 1 & & & & -i & & & & -1 & & & & i & \\
 & & & 1 & & & & -i & & & & -1 & & & & i
\end{array}\right]. \tag{14}$$

In this way the full transform requires only 8 complex multiplications (or the equivalent of 6 if we use that w^2 and w^6 have real and imaginary parts equal). This should be compared to 256 complex multiplications in the most straightforward implementation of (11).

ACKNOWLEDGMENTS

I wish to thank Professors H. B. Keller and P. G. Saffman for helpful and encouraging discussions and the referees for a large number of important suggestions.

REFERENCES

1. G. K. BATCHELOR, "Theory of Homogeneous Turbulence," p. 186, University Press, Cambridge, England, 1953.
2. G. K. BATCHELOR, Computation of the energy spectrum in homogeneous two-dimensional turbulence, *Phys. Fluids Suppl.* **2** (1969), 233–239.
3. E. O. BRIGHAM, "The Fast Fourier Transform," Prentice–Hall, Englewood Cliffs, N.J., 1974.
4. J. W. COOLEY, P. A. W. LEWIS, AND P. D. WELCH, The Fast Fourier Transform and Its Applications, *IEEE Trans. Educ.* **E-12**, No. 1 (1969), 27–34.
5. J. W. COOLEY, P. A. W. LEWIS, AND P. D. WELCH, The Fast Fourier Transform algorithm: Programming considerations in the calculation of sine, cosine and Laplace transforms, *J. Sound Vib.* **12** (1970), 315–337.
6. J. W. COOLEY AND J. W. TUKEY, An algorithm for the machine calculation of complex Fourier series, *Math. Comp.* **19** (1965), 297–301.
7. G. S. DEEM AND N. J. ZABUSKY, Ergodic boundary in numerical simulations of two-dimensional turbulence, *Phys. Rev. Lett.* **27** (1971), 396–399.

8. B. FORNBERG, On a Fourier method for the integration of hyperbolic equations, *SIAM J. Numer. Anal.* **11** (1975), 509–528.
9. D. G. FOX AND S. A. ORSZAG, Pseudospectral approximation to two-dimensional turbulence, *J. Comp. Phys.* **11** (1973), 612–619.
10. J. GAZDAG, "Time-Differencing Schemes and Transform Methods," IBM Palo Alto Scientific Center Technical Report No. G320-3330 (1975).
11. J. A. GLASSMAN, A generalization of the fast Fourier transform, *IEEE Trans. Computers* C-19, No. 2 (1970), 105–116.
12. J. R. HERRING, S. A. ORSZAG, R. H. KRAICHMAN, AND D. S. FOX, Decay of two-dimensional homogeneous turbulence. *J. Fluid Mech.* **66**, part 3 (1974), 417–444.
13. R. H. KRAICHNAN, Inertial ranges in two-dimensional turbulence, *Phys. Fluids* **10**, No. 7 (1969), 1417–1423.
14. H.-O. KREISS AND J. OLIGER, Comparison of accurate methods for the integration of hyperbolic equations, *Tellus* **24** (1972), 199–215.
15. C. E. LEITH, Diffusion approximation for two-dimensional turbulence, *Phys. Fluids* **11** (1968), 671–673.
16. D. K. LILLY, Numerical simulation of two-dimensional turbulence, *Phys. Fluids Suppl.* **2** (1969), 240–249.
17. D. K. LILLY, Numerical simulation on developing and decaying two-dimensional turbulence, *J. Fluid Mech.* **45** (1971), 395–415.
18. L. ONSAGER, "Statistical Hydrodynamics," Supplemento A1, Vol. VI, Serie IX Del Nuovo Cimento, N. 2 (1949), pp. 279–287.
19. S. A. ORSZAG AND M. ISRAELI, Numerical simulation of viscous incompressible flow, *Annu. Rev. Fluid Mech.* **6** (1974), 281–318.
20. N. A. PHILLIPS, "An Example of Non-linear Computational Instability, The Atmosphere and the Sea in Motion" (B. Bolin, Ed.), pp. 501–504, Rockefeller Institute, New York, 1959.
21. P. G. SAFFMAN, "Lectures on Homogeneous Turbulence, Topics in Nonlinear Physics" (N. J. Zabusky, Ed.), pp. 485–614, Springer–Verlag, Berlin/Heidelberg, 1968.
22. P. G. SAFFMAN, On the spectrum and decay of random two-dimensional vorticity distributions at large Reynolds number, *Stud. Appl. Math.* **50** (1971), 377–383.
23. C. E. SEYLER, Y. SALU, D. MONTGOMERY, AND G. KNORR, Two-dimensional turbulence in inviscid fluids or guiding center plasmas, *Phys. Fluids* **18** (1975), 803–813.